Extensivity and additivity of the Kolmogorov-Sinai entropy for simple fluids

Moupriya Das,[1] Anthony B. Costa,[2] and Jason R. Green[1,3,4,*]

[1]*Department of Chemistry, University of Massachusetts Boston, Boston, Massachusetts 02125, USA*

[2]*Numerical Solutions, Inc., P.O. Box 396, Corvallis, Oregon 97330, USA*

[3]*Department of Physics, University of Massachusetts Boston, Boston, Massachusetts 02125, USA*

[4]*Center for Quantum and Nonequilibrium Systems, University of Massachusetts Boston, Boston, Massachusetts 02125, USA*

(Received 28 September 2016; published 3 February 2017)

According to the van der Waals picture, attractive and repulsive forces play distinct roles in the structure of simple fluids. Here, we examine their roles in dynamics; specifically, in the degree of deterministic chaos using the Kolmogorov-Sinai (KS) entropy rate and the spectra of Lyapunov exponents. With computer simulations of three-dimensional Lennard-Jones and Weeks-Chandler-Andersen fluids, we find repulsive forces dictate these dynamical properties, with attractive forces reducing the KS entropy at a given thermodynamic state. Regardless of interparticle forces, the maximal Lyapunov exponent is intensive for systems ranging from 200 to 2000 particles. Our finite-size scaling analysis also shows that the KS entropy is both extensive (a linear function of system-size) and additive. Both temperature and density control the "dynamical chemical potential," the rate of linear growth of the KS entropy with system size. At fixed system-size, both the KS entropy and the largest exponent exhibit a maximum as a function of density. We attribute the maxima to the competition between two effects: as particles are forced to be in closer proximity, there is an enhancement from the sharp curvature of the repulsive potential and a suppression from the diminishing free volume and particle mobility. The extensivity and additivity of the KS entropy and the intensivity of the largest Lyapunov exponent, however, hold over a range of temperatures and densities across the liquid and liquid-vapor coexistence regimes.

DOI: 10.1103/PhysRevE.95.022102

I. INTRODUCTION

Statistical mechanics predicts the emergent behavior of systems both at and away from equilibrium. Though more established at equilibrium than away from it [1], there are promising results for nonequilibrium processes drawing from dynamical systems theory [2,3]. The central quantities include the Lyapunov exponents and Kolmogorov-Sinai entropy per unit time (or simply KS entropy) [4,5]. Both quantities are signatures of deterministic chaos [6,7]: the former measure the exponential rate at which initially close trajectories diverge, and the latter is the rate of phase-space mixing, with applications in statistical mechanics dating back to Krylov [8]. In constructing a nonequilibrium statistical mechanical theory from these dynamical observables, it would be ideal to have equilibrium statistical mechanics as a limiting case. Thus, the equilibrium properties of the KS entropy we study here are relevant to its use away from equilibrium.

While the KS entropy is technically a rate, given its name, it is tempting to look for similarities and quantitative connections with the thermodynamic entropy, or the entropy production (rate), a line of reasoning that has yielded important results [9–11]. Two key features of the thermodynamic entropy are its linear growth with system size, or extensivity, and its additivity [12,13]. The KS entropy is extensive in time, but surveying discrete dynamical systems (e.g., the tent and logistic maps [14]) and models of physical systems (e.g., symmetric exclusion processes, random walks with absorbing boundaries, and an infinite-range Ising model with spin-flip dynamics [15]), there is no guarantee that the KS entropy is extensive in system size. Furthermore, compared to its system-size extensivity, the additivity of the KS entropy seems to have been addressed less frequently [16]. Here, we analyze both the additivity and extensivity of the KS entropy for simple fluids over a range of system sizes that avoids corruption from finite-size effects.

Many aspects of Lyapunov exponents and the KS entropy have been considered over the past few decades [16–47]. However, because of the computational expense, calculations of the full Lyapunov spectra and the KS entropy are typically limited to systems with few degrees of freedom or short times scales [48]. This expense can be offset by simplifying the model; for example, hard-disks and hard spheres are a common choice, and they have the added advantage that there are well-established equilibrium statistical mechanical theories [28–33]. Models with soft interactions, though, such as the Lennard-Jones (LJ) potential, are computationally more demanding [34]. In this case, it is often necessary to instead sacrifice the number of real spatial dimensions, working in one or two dimensions instead of three [34–41]. For those simulations calculating the complete Lyapunov spectrum in three-dimensional systems, the largest number of particles considered was on the order of hundreds [42–46], which the present authors extended to over 1000 [48]. Part of the goal in this work is to extend the largest system size (up to 2000) for which the Lyapunov spectrum is available for simple fluids and to test the extensivity and additivity of the KS entropy through finite-size scaling.

In this work, we compute the KS entropy and the Lyapunov spectrum from molecular dynamics simulations [49] of Lennard-Jones and Weeks-Chandler-Andersen fluids [50,51]. We systematically analyze the temperature and density dependence of these dynamical observables for three-dimensional fluids, which is only currently known for two-dimensional systems [37,39]. Our scaling analysis of the KS entropy

*jason.green@umb.edu

and Lyapunov spectra with the number of particles in these fluids adds to previous work on the scaling of the largest Lyapunov exponent [16,42,44] and studies of small (less than 100 particles) three-dimensional systems [42,44]. Overcoming the significant computational difficulty that has prevented finite-size scaling over a wide range of system sizes raises the question of whether the KS entropy is, in fact, extensive. We address this question here, as well as how the nature of the interparticle interactions, temperature, and density, affect this scaling.

II. MODEL SYSTEMS AND COMPUTATIONAL METHODS

We consider classical, three-dimensional, periodic fluids containing N particles with $3N$ positions and $3N$ momenta. The Hamiltonian of the system is $H(\tilde{r}_{ij},\tilde{p}_k) = \sum_k^{3N} \tilde{p}_k^2/2m + \sum_{i<j}^{N} V(\tilde{r}_{ij},\tilde{t})$, with the interaction potential $V(\tilde{r}_{ij})$ between the particles i and j a distance, $\tilde{r}_{ij}$, apart. One type of fluid we consider consists of particles interacting pairwise through the Lennard-Jones potential (LJ) [52],

$$V_{\mathrm{LJ}}(\tilde{r}_{ij}) = 4\epsilon_{ij}\left[\left(\frac{\sigma}{\tilde{r}_{ij}}\right)^{12} - \left(\frac{\sigma}{\tilde{r}_{ij}}\right)^{6}\right]. \tag{1}$$

The parameter ϵ corresponds to the strength of the interaction between particles i and j. All interactions are identical so that we model a single-component fluid. The first term of the potential is a repulsive contribution to pairwise interactions, which operates over short distances. The second term is an attractive contribution acting over a comparatively longer range. The parameter σ is the distance at which the attractive and the repulsive contributions to the potential are equal and is a measure of the particle size. To understand the influence of the attractive and repulsive interactions on the KS entropy, we also consider a fluid consisting of particles that interact through the Weeks-Chandler-Andersen (WCA) potential [53]. The WCA potential is

$$V_{\mathrm{WCA}}(\tilde{r}_{ij}) = \begin{cases} V_{\mathrm{LJ}}(\tilde{r}_{ij}) + \epsilon & \text{if} \quad \tilde{r}_{ij} < 2^{1/6}\sigma \\ 0 & \text{if} \quad \tilde{r}_{ij} \geqslant 2^{1/6}\sigma. \end{cases} \tag{2}$$

Both interparticle interactions are shown in Fig. 1(a).

We simulate constant energy trajectories of the periodic LJ and WCA fluids in three dimensions with molecular dynamics. We work in LJ reduced units with distance $r = \tilde{r}/\sigma$, density $\rho = \tilde{\rho}\sigma^3$, temperature $T = k_B\tilde{T}/\epsilon$, time $t = \tilde{t}/\sqrt{m\sigma^2/\epsilon}$, and KS entropy $h_{\mathrm{KS}} = \tilde{h}_{\mathrm{KS}}\sqrt{m\sigma^2/\epsilon}$. All particles have unit mass, and, unless noted otherwise, ϵ and σ are also unity. All results shown here are from constant energy trajectories. The initial phase points for these trajectories, however, were sampled from a canonical ensemble with temperature T using a Berendsen thermostat with a time constant of 0.5. The constant energy trajectories evolve in time according to the velocity Verlet algorithm with time step $\Delta t = 10^{-3}$. We both shift and truncate interparticle forces [54] for a Verlet list with a cutoff and a "skin" of 0.1σ. The cutoff was 2.5σ for the LJ fluid and $2^{1/6}\sigma$ for the WCA fluid.

Together with each constant energy trajectory we simulate the tangent space dynamics. These dynamics impose significant computational limitations on the largest system sizes that are accessible. For each constant energy trajectory, the Lyapunov exponents and the KS entropy, h_{KS}, are calculated from the set of orthogonal Lyapunov basis vectors (Gram-Schmidt vectors) [55,56]. The mth vector elements are the first variations in position and momentum $(\delta q_{mn},\delta p_{mn})^T$ with $m,n = 1,\ldots,6N$. These vectors are evolved according to the linearized Hamiltonian dynamics [55], along with the phase point, using to the linearized velocity Verlet algorithm and orthonormalization at every step [48,57–59]. During the evolution, the first vector orients parallel to the maximally changing tangent space direction. Regular orthonormalization avoids the collapse of the remaining vectors onto the maximally changing direction. The linearized velocity Verlet form of the tangent space propagator requires the second derivative (Hessian) matrices at consecutive steps. We use forward differences of the analytical gradients with a displacement of 10^{-4}. Initial basis sets are randomly filled, orthonormal matrices. All calculations were in single precision.

During the simulation, the Lyapunov spectrum is calculated from the set of orthogonal Lyapunov vectors at every time step [17]. We calculate the full Lyapunov spectrum using the metric $|\delta x_n|^2 = \sum_m^{6N}[\delta q_{mn}(t)^2 + \delta p_{mn}(t)^2]$. The nth finite-time Lyapunov exponent is

$$\lambda_n(t,t_0) = |t - t_0|^{-1} \ln \frac{|\delta x_n(t)|}{|\delta x_n(t_0)|}. \tag{3}$$

According to Pesin's theorem [6], for closed dynamical systems, the KS entropy, h_{KS}, is the sum of the positive Lyapunov exponents, $\sum_n^+ \lambda_n$, in the infinite-time limit. To calculate statistical errors for h_{KS} and $\lambda_{\max}$ from long, but finite, simulations, we neglect the initial transient of the Lyapunov exponents and use the standard deviation of the remaining time series.

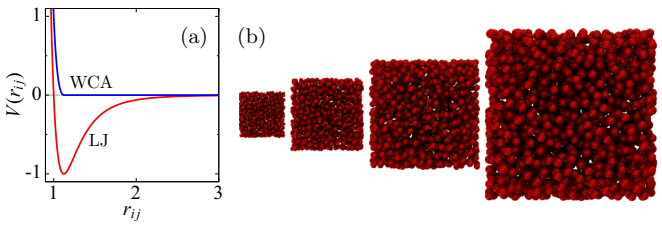

FIG. 1. (a) Interaction potential between the ith and jth particle. (b) Snapshots of 4 out of the 15 system sizes we simulate with NVE molecular dynamics: N = 200, 300, 400, 500, 600, 700, 800, 900, 1000, 1100, 1300, 1500, 1700, 1900, and 2000.

III. RESULTS AND DISCUSSION

A. System-size scaling of the Lyapunov spectrum and the KS entropy

From simulations of many-particle systems in one, two, and three dimensions [16,20,39,40], there is accumulating numerical evidence that the Lyapunov spectrum is well-defined in the thermodynamic limit: $N, V \to \infty$ such that $\rho = N/V$ is constant. Whether chaos persists with a well-defined Lyapunov spectrum in scaling limits is also of interest in generic dynamical systems [60]. If a thermodynamic limit exists, the structure of the spectrum is a global property of the

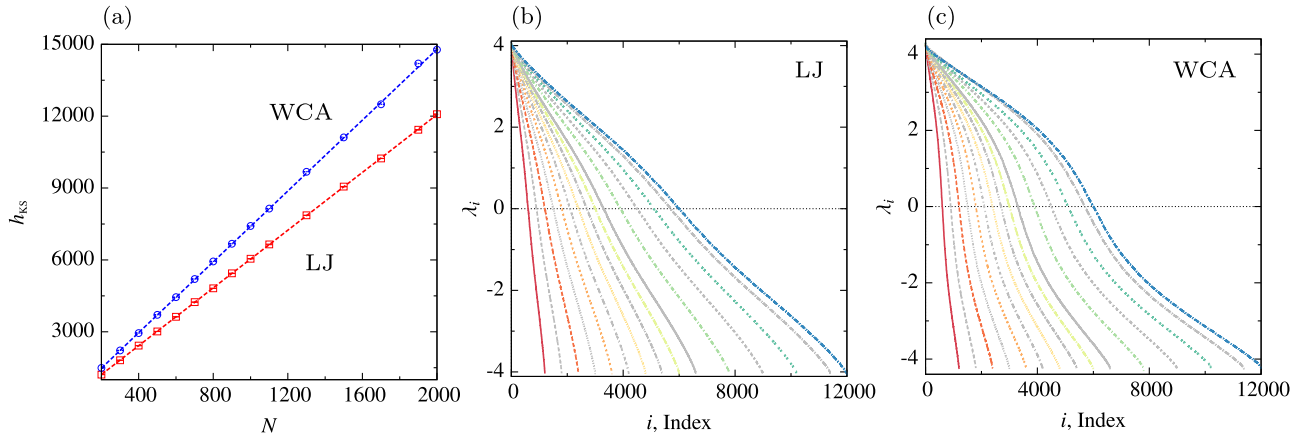

FIG. 2. (a) Representative data showing the KS entropy is linearly extensive in system size, N, for both Lennard-Jones (□) and Weeks-Chandler-Andersen (○) fluids. Data points with error bars are from simulations at fixed number density, $\rho = 0.75$, and a kinetic temperature of approximately $T = 0.9$. Linear fits of the data (dashed lines) give $h_{KS} = 6.0276\,N + 8.6698$ with correlation coefficient 0.999992 for LJ and $h_{KS} = 7.4104\,N + 1.1900$ with correlation coefficient 0.999943 for WCA. The quality of these fits supports the extensivity of the KS entropy over an order of magnitude in N. The shallow slope of $h_{KS}(N)$ for the LJ fluid compared to the purely repulsive WCA fluid is due to the attractive forces. The associated Lyapunov spectra of the (b) LJ and (c) WCA fluids with $N = 200$, 300, 400, 500, 600, 700, 800, 900, 1000, 1100, 1300, 1500, 1700, 1900, and 2000 particles at $\rho = 0.75$ and $T = 0.9$. The KS entropy is the area under the positive portion of the spectra. For each spectrum, the symmetry about the horizontal axis is a consequence of the conjugate pairing rule.

dynamics at equilibrium. The spectral structure is important, in part, because it determines the thermodynamic scaling properties of the KS entropy.

To understand the scaling of the KS entropy with system size, we simulate a set of 15 systems with the number of particles varying from 200 to 2000 [Fig. 1(b)]. From our NVE simulations, we find the KS entropy scales linearly with the number of particles, N [Fig. 2(a)]. This result spans a range of temperatures and densities that include pure liquids and coexisting phases for both Lennard-Jones and Weeks-Chandler-Andersen systems. The representative data in Fig. 2 are finite-size scaling results where the number of particles extends over an order of magnitude at fixed number, $\rho = N/V = 0.75$, and energy density, $E/N = -2.9304$ for the LJ fluid and $E/N = 1.9714$ for the WCA fluid. At this energy density, the average kinetic temperature is 0.9 and corresponds to the conditions of the pure liquid phase [61]. The (kinetic) temperature is calculated from the equipartition theorem, $T = 2\langle E_{kin}\rangle/3Nk_B$, with the average kinetic energy per particle.

Trajectories of simple fluids disperse because of the convexity of the interatomic interaction potential. This Lyapunov instability of the dynamics also depends on the degree of curvature of the potential, as is known, for example, from studies of isolated molecules and clusters [62–64]. In the van der Waals picture of fluids, one expects the short range of the steep repulsive wall to contribute more to the dynamical instability than the slowly varying, long-ranged attractions between particle pairs. These competing forces are manifest in the dynamics through both the KS entropy shown in Fig. 2(a) and the Lyapunov spectra shown in Figs. 2(b) and 2(c). Both the LJ and WCA fluids have identical thermodynamic conditions, a number density of $\rho = 0.75$, and a kinetic temperature around $T = 0.9$, to isolate the effect of the attractive and repulsive interactions. These data show that the scaling of h_{KS} with N is linear for both LJ and WCA fluids, despite "turning off" attractive forces. Also apparent in these data is the higher h_{KS} for the WCA fluid over this range of system sizes. This finding reflects the van der Waals picture and our intuition about the steepness of the repulsive wall; roughly speaking, attractive forces slow down the dispersion of trajectories, while repulsive interactions hasten their divergence. More quantitatively, the relative error of the KS entropy $|h_{KS}^{WCA} - h_{KS}^{LJ}|/h_{KS}^{WCA} \times 100$ is between 17 and 19% for all N. Ultimately, this behavior of the exponents and h_{KS} can be linked to their dependence on the curvature of interaction potential through the Hessian [17]. Building on these ideas, we expect the number of pairs sampling the attractive and repulsive portions of the potential to affect the global KS entropy. For example, in a 1000 particle system, a given LJ particle experiences roughly 6 repulsive and 54 attractive interactions on average at $\rho = 0.75$ and $T = 0.9$. Under the same conditions, a particular WCA particle has roughly six repulsive neighbors.

The structure of the Lyapunov spectrum underlies the linear growth of the KS entropy with system-size. Figures 2(b) and 2(c) show the complete Lyapunov spectra for LJ and WCA fluids, respectively. The spectra are symmetric as expected from the conjugate pairing rule [65] and Liouville's theorem. However, comparing Figs. 2(b) and 2(c) shows that the Lyapunov spectra of these fluids differ significantly in their structure at this temperature and density. The spectrum of the LJ fluid is nearly a linearly decreasing function, $\lambda_i \approx \lambda_{max}(1 - i/L)$, of the index, $i = 0, \ldots, L = 3N - M$. The Lyapunov exponents are in descending order. For M conserved quantities, $2M$ Lyapunov exponents are zero [39]. For a Lyapunov spectrum with a linear structure, there is a geometrical relationship between the maximal exponent and the KS entropy; when the spectrum decreases linearly with the index, the positive half of the Lyapunov spectrum is a right triangle with a base $3N$, height λ_{max}, and area h_{KS}. The area is then $h_{KS} = 3N\lambda_{max}/2$, resembling the equipartition theorem for energy $\langle E_{kin}\rangle = 3Nk_BT/2$ with the role of k_BT

being played by $\lambda_{\max}$. This analogy extends even further since $\lambda_{\max}$ and T are both intensive quantities.

The association of the KS entropy with the area of the positive portion of the Lyapunov spectrum is valid regardless of the spectral structure, but the relationship $h_{\rm KS} = 3N\lambda_{\max}/2$ only strictly holds for the special case of a spectrum of the form $\lambda_i = \lambda_{\max}(1 - i/L)$. However, if the largest Lyapunov exponent, $\lambda_{\max}$, is intensive then this simple geometrical relation supports the linear extensivity of $h_{\rm KS}$. To see this connection, if $\lambda_{\max}$ is independent of N then $h_{\rm KS} = c\,N$ with a constant $c = 3\lambda_{\max}/2$. In other words, the base of the triangle alone will linearly grow the area, KS entropy. While this geometrical argument assumes an exactly linear spectrum, it correctly describes the extensivity of the KS entropy in the LJ fluid despite small nonlinearities seen in Fig. 2(b), and the strong deviations from linearity in the WCA spectrum. In fact, we find $h_{\rm KS}$ scales linearly with N for both LJ and WCA under all the conditions we have studied. We have suppressed notation, but the form of the Lyapunov spectrum and the rate of divergence of $h_{\rm KS}$ with N depend on the density and temperature. And, as we will show, the spectra do deviate significantly from linear under some thermodynamic conditions.

The extensivity of the KS entropy depends on the system-size scaling of the largest Lyapunov exponent. Using the geometrical argument above, if $\lambda_{\max}$ is constant, as found by Posch and Hoover [42,44] for three-dimensional systems, then $h_{\rm KS}$ is a linear function of N. But, if $\lambda_{\max}$ instead has a weak logarithmic divergence, $\ln N$, as suggested by Searles, Evans, Isbister [16] then $h_{\rm KS}$ will scale as $N \ln N$. It is noteworthy that Searles *et al.* also observed deviations from this logarithmic scaling $\mathcal{O}(1/N)$ for small system sizes. We see neither finite-size effects nor any trend in the largest exponent with system size. This finding is supported by the data in Figs. 2(b) and 2(c) and a closer analysis where we found no clear trends in the maximum Lyapunov exponent with system size within our statistical errors. Our data, over an order of magnitude of system sizes with high-quality linear fits, are strong numerical evidence of the extensivity of $h_{\rm KS}$ and intensivity of $\lambda_{\max}$.

From the Lyapunov spectra in Fig. 2(b), we can infer a thermodynamic limit for their structure. The modulus of the linear slope of the spectra is $\lambda_{\max}/3N \approx 1/N$, since the magnitude of $\lambda_{\max}$ is around 4. We confirmed this scaling of the slope for the data shown. This result will likely hold for sufficiently large N even if the largest exponent has a weak logarithmic divergence as suggested by Searles *et al.* Since $\lambda_{\max} \approx \ln N$ diverges more slowly than $3N$, the slope will be $\lambda_{\max}/3N \sim N^{-1} \ln N$ for $N > 1$. Assuming this relation continues to hold in the large system limit, as N, $h_{\rm KS} \to \infty$, the slope will tend asymptotically to zero and the Lyapunov spectrum will be uniform.

The KS entropy is clearly extensive, meaning it scales linearly with the number of particles in the system such that there is a finite density, $h_{\rm KS}/N$, in the thermodynamic limit. These data also show that the KS entropy is additive. Loosely speaking, the KS entropy will double upon doubling the system size. More generally, KS entropy of each system with size N is an additive function of the KS entropies for any (say, two) subsystems with sizes N_A and N_B such that $N = N_A + N_B$. Mathematically, $h_{\rm KS}(N) = h_{\rm KS}(N_A) + h_{\rm KS}(N_B)$. For example, the KS entropy of a 600-particle composite system is the sum of the KS entropies of a 200 particle and a 400 particle system with less than 0.5% error in our data. We verified this property for all possible composite systems and their associated subsystem partitions with our data up to $N = 2000$ for both LJ and WCA fluids. The error is less than 0.5% in all cases.

In sum, these data show that the KS entropy is additive and extensive for simple fluids, like the thermodynamic entropy. To justify the linear scaling of $h_{\rm KS}$ against N from the thermodynamic point of view, we can compare its behavior to that of the thermodynamic entropy S. From the fundamental relation, $dS = dU/T + P\,dV/T - \mu\,dN/T$, the chemical potential determines the dependence of the thermodynamic entropy on system size, $(\partial S/\partial N)_{U,V} = -\mu/T$ in the microcanonical ensemble, assuming the thermodynamic state is not on a phase boundary or at a critical point. The negative value of μ determines the rate of linear growth of S with N for homogeneous, single component systems at fixed temperature. From this perspective, the linear scaling of $h_{\rm KS}$ against N is consistent with thermodynamics. If we were to take this analogy further, the slope of the KS entropy versus N would be $-\mu_{\rm KS}/T$. In the next subsection, we will see how temperature affects $\partial h_{\rm KS}/\partial N$.

It is worth noting that while the KS entropy and the thermodynamic entropy are not equivalent, given that their dimensions differ, their common properties are of interest to further establish links between the theories of dynamical systems and liquids. Of course, the Lennard-Jones and Weeks-Chandler-Andersen systems we study here are at equilibrium, and their typical microscopic states will be those that maximize entropy. A positive KS entropy rate for these many-particle systems does not imply a positive macroscopic entropy production rate. Rather, being the sum of only the positive Lyapunov exponents, it measures the extent of dynamical randomness at the microscopic level that is not apparent at the macroscopic level. In contrast, the sum of all Lyapunov exponents can be linked to the entropy production rate of nonequilibrium thermodynamics [2]. But here, because the systems are isolated, Liouville's theorem ensures the conservation of phase space volume and that this sum is strictly zero [Fig. 2(b)], which is consistent with these systems being at equilibrium, and, so, producing no entropy on a macroscopic scale.

B. Temperature dependence of the Lyapunov spectrum and the KS entropy

The structure of the Lyapunov spectrum and the rate of linear divergence of $h_{\rm KS}$ with N depend on both temperature and density. To understand their temperature dependence, we focus on LJ and WCA fluids with 1000 particles. Again, in practice, we sample initial phase points from the canonical ensemble, T, and show results from subsequent constant energy trajectories with a kinetic temperature $T_{\rm kin} = T$. In the latter, the total energy is such that the kinetic temperature equilibrates around the temperature in the preceding NVT simulation. The initial configurations of the NVE trajectories were sampled after complete thermal equilibration, as evidenced by stationary

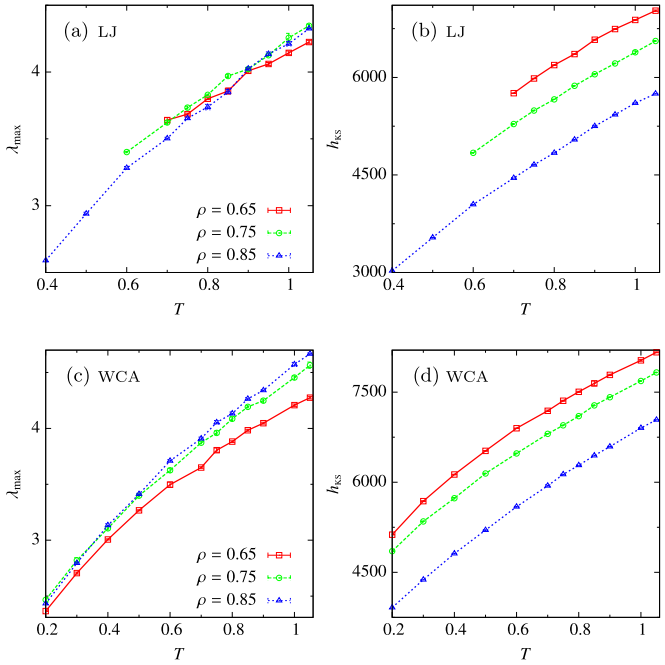

FIG. 3. (a) The largest Lyapunov exponent, λ_{max}, and (b) the KS entropy, h_{KS}, as a function of temperature T for the LJ fluid at $\rho = 0.65$, 0.75, and 0.85. (c) λ_{max} and (d) h_{KS} as a function of temperature for the WCA fluid at the same number densities. The number of particles is fixed $N = 1000$. Statistical errors are smaller than the symbol size.

values of the temperature during the NVT simulations, and the absence of visual signs of phase coexistence. The largest Lyapunov exponent λ_{max} as a function of temperature T is shown in Figs. 3(a) and 3(c) for the LJ and WCA fluids, respectively. In both cases, λ_{max} increases monotonically with the kinetic temperature T. The KS entropy shown in Figs. 3(b) and 3(d) also increases monotonically.

For all densities studied, the temperature dependence of both λ_{max} and h_{KS} is monotonic. Irregularities appear for the LJ system at low temperatures, below $T = 0.7$, 0.6, and 0.4, for densities $\rho = 0.65$, 0.75, and 0.85, respectively. This irregularity is apparent in both λ_{max} and h_{KS} as a function of T, and is the result of crossing the liquid-vapor or solid-vapor phase boundary [61]. We confirmed the presence of two phases by visually inspecting the sampled configurations at these conditions. Therefore, in Figs. 3(a) and 3(b) and throughout, we only present λ_{max} and h_{KS} for the LJ systems over the temperature range where we see no signs of phase coexistence and the temperature dependence is smooth and monotonic.

At densities $\rho = 0.75$ and 0.85, the LJ fluid is mostly a pure liquid (above $T = 0.7$) in the temperature range where λ_{max} and h_{KS} vary regularly with temperature. For $\rho = 0.65$ the liquid regime begins at a higher temperature ($T = 0.9$). These data suggest that the regular behavior of λ_{max} and h_{KS} with T are a signature of the fluid phase of the LJ system. The temperature dependence of λ_{max} and h_{KS} was reported to be $\sqrt{T}$ for two-dimensional WCA systems [37]. Our regression analysis of the temperature dependence for three-dimensional LJ fluids, however, was inconclusive. The linear correlation coefficients of the data of λ_{max} and h_{KS} against T and $\sqrt{T}$ are greater than 0.995 in this higher band of temperature. As the LJ system has extended coexistence regions, the liquid state only exists over a narrow window of temperatures, which hinders a full resolution of the temperature dependence of λ_{max} and h_{KS}.

By comparison, the trends of both λ_{max} and h_{KS} are more regular functions of temperature for the WCA fluid. For WCA, both the largest Lyapunov exponent and KS entropy scale as $\sqrt{T}$ for these three densities. The linear correlation coefficients of the data λ_{max} and h_{KS} against $\sqrt{T}$ have values greater than 0.987. For λ_{max}, this finding is in agreement with previous simulations in two dimensions [37]. Physically, the monotonic increase of these observables with temperature agrees with the intuition that raising the temperature enhances particle mobility and consequently expedites the divergence of trajectories. There has been a discussion of how to make this intuition quantitative [22–24].

The temperature dependence of the full Lyapunov spectrum underlies the KS entropy. Lyapunov spectra, normalized by λ_{max}, are shown in Figs. 4(a)–4(f) for both LJ and WCA fluids. There is a clear tendency of the spectra toward linearity at higher densities. With increasing density, the temperature dependence of the spectra is also suppressed—there is less spread. Above temperature $T = 0.7$, for all densities, the spectra do not vary significantly with temperature. A likely cause of this loss of spectral structure at higher temperatures is the emergence of the fluid phase (pure liquid or liquid-vapor coexistence) for the LJ system. When the fluid phase, especially the pure liquid phase, is present, the temperature dependence is weak. Figures 5(a) and 5(b) show the temperature dependence of the ratio $2h_{KS}/3N\lambda_{max}$ for the LJ and WCA fluids. The ratio varies to a small extent above $T = 0.7$. Above this temperature the KS entropy and Lyapunov spectra mostly reflect the dynamics of the pure fluids.

An important technical consideration in the molecular simulation of fluids is the cutoff range of the interaction potential, r_c. The choice of length scale can strongly affect equilibrium properties, e.g., the location of phase boundaries [61]. Truncating and shifting the potential affects the energy scale. To examine the influence of a truncated and shifted interaction potential on the KS entropy rate, we investigated the scaling of h_{KS} with the number of particles for different cutoff. Changing the cutoff from $r_c = 2.5\sigma$ to $r_c = 5.0\sigma$, but keeping all other properties fixed (viz., number density and kinetic temperature), we repeated our calculations of the KS entropy for $N = 800$ to 2000 LJ particles. We found the KS entropy versus N was identical, within statistical errors, to the data in Fig. 2(a) with a cutoff distance of 2.5σ. To a certain extent, we do not expect the cutoff to dramatically affect the KS entropy, since this portion of the potential plays a small role in the dynamics at these densities and temperatures. The average interparticle separation varies between 3.3 to 2.4 within the density range 0.4 to 0.9 in the temperature range we consider.

Upon increasing the temperature, we find the KS entropy has a larger magnitude and diverges more rapidly with N, again at fixed E/N and N/V. This finding is not surprising from an analogy with the thermodynamics of single-component systems, where the steeper slope of the h_{KS} with N suggests $\partial h_{KS}/\partial N = -\mu_{KS}(T)/T$ is positive when $\mu_{KS} < 0$. The linear extensivity of the KS entropy enables us to interpret the

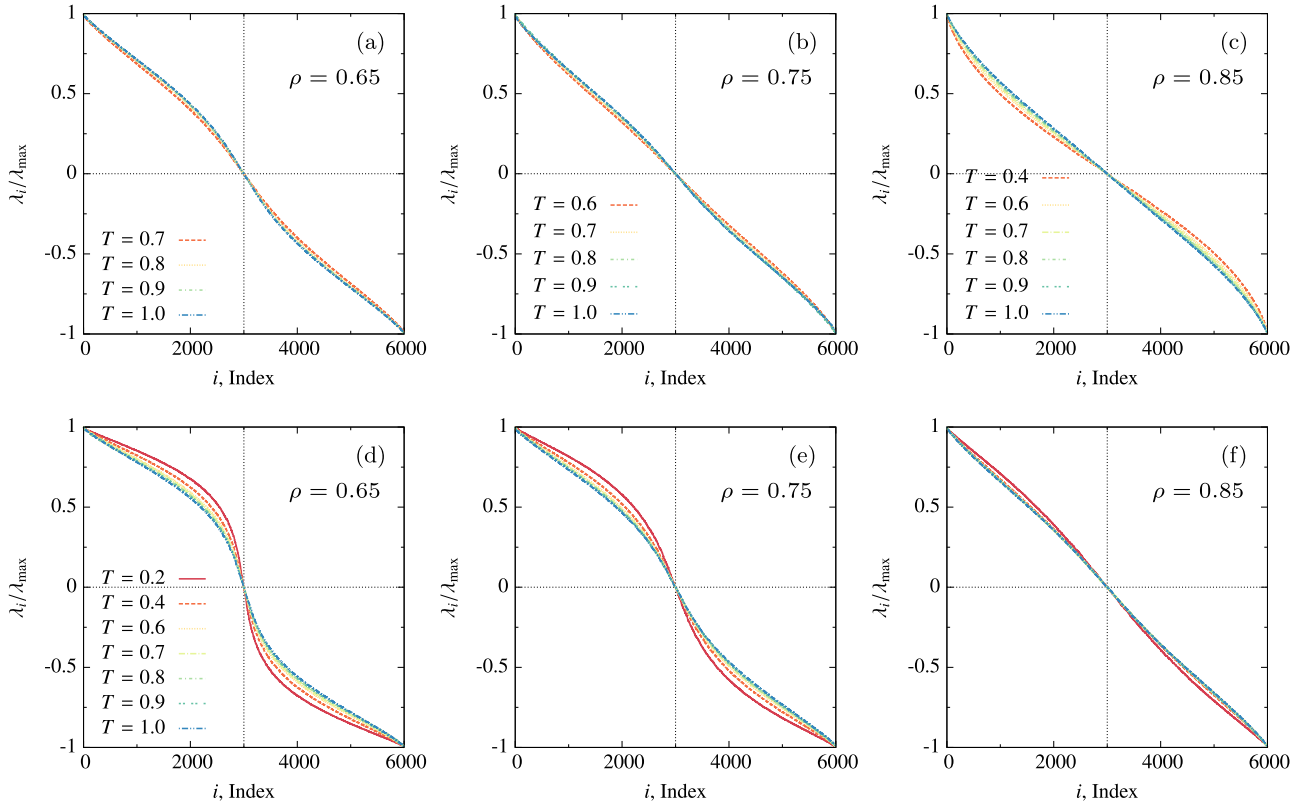

FIG. 4. Normalized Lyapunov spectra, λ_i/λ_{max}, for the (a–c) LJ and (d–f) WCA fluid for a range of kinetic temperatures and densities (a, d) $\rho = 0.65$, (b, e) $\rho = 0.75$, and (c, f) $\rho = 0.85$. The number of particles is fixed, $N = 1000$.

constant slope as an intensive chemical potential, $\mu_{KS}(T)$. For now, we simply point out this agreement with thermodynamics and leave for future work whether the chemical potential estimated from the KS entropy relates to the thermodynamic chemical potential.

Temperature (and density) control the rate of divergence of h_{KS} with N. Evidence is shown in Fig. 6(a), showing the KS entropy for the LJ fluid from $N = 800$ to 2000 particles at $\rho = 0.75$ and three different temperatures. For all three temperatures, the KS entropy scales linearly with N, with a steeper slope at higher temperatures. We also examined the effect of density on the variation of h_{KS} against N for three densities and at $T = 0.9$ for the LJ fluid [Fig. 6(b)]. From the data in Figs. 3(a)–3(d), the temperature dependence of the largest exponent and the KS entropy is also sensitive to density. Figure 6(b) also suggests density affects the KS entropy scaling with N. The slope of h_{KS} with N for varying densities also agrees with thermodynamic intuition (increasing density leads to an increase in the chemical potential and lowering of rate of divergence of h_{KS} with N) and physical intuition (increasing density decreases particle mobility and the magnitude of h_{KS}). We now turn to the density dependence of λ_{max} and the KS entropy.

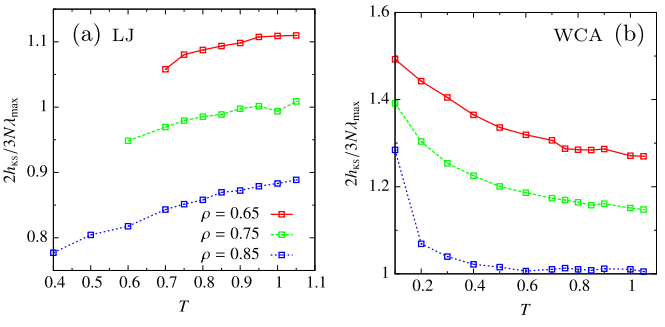

FIG. 5. The function $2h_{KS}/3N\lambda_{max}$ against temperature T at three different number densities for (a) the LJ fluid and (b) the WCA fluid. For both the cases, $N = 1000$.

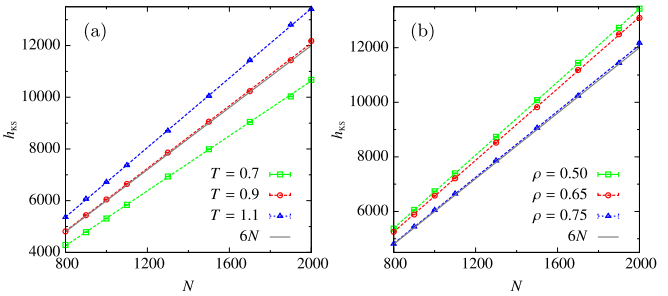

FIG. 6. (a) The KS entropy, h_{KS}, as a function of the number of particles, N, for the Lennard-Jones fluid at (a) three temperatures ($\rho = 0.75$) and (b) three densities ($T = 0.9$). Data points with error bars smaller than symbols are from simulations at fixed number density. Dashed lines are linear fits. The function $6N$ (solid black line) is shown for reference.

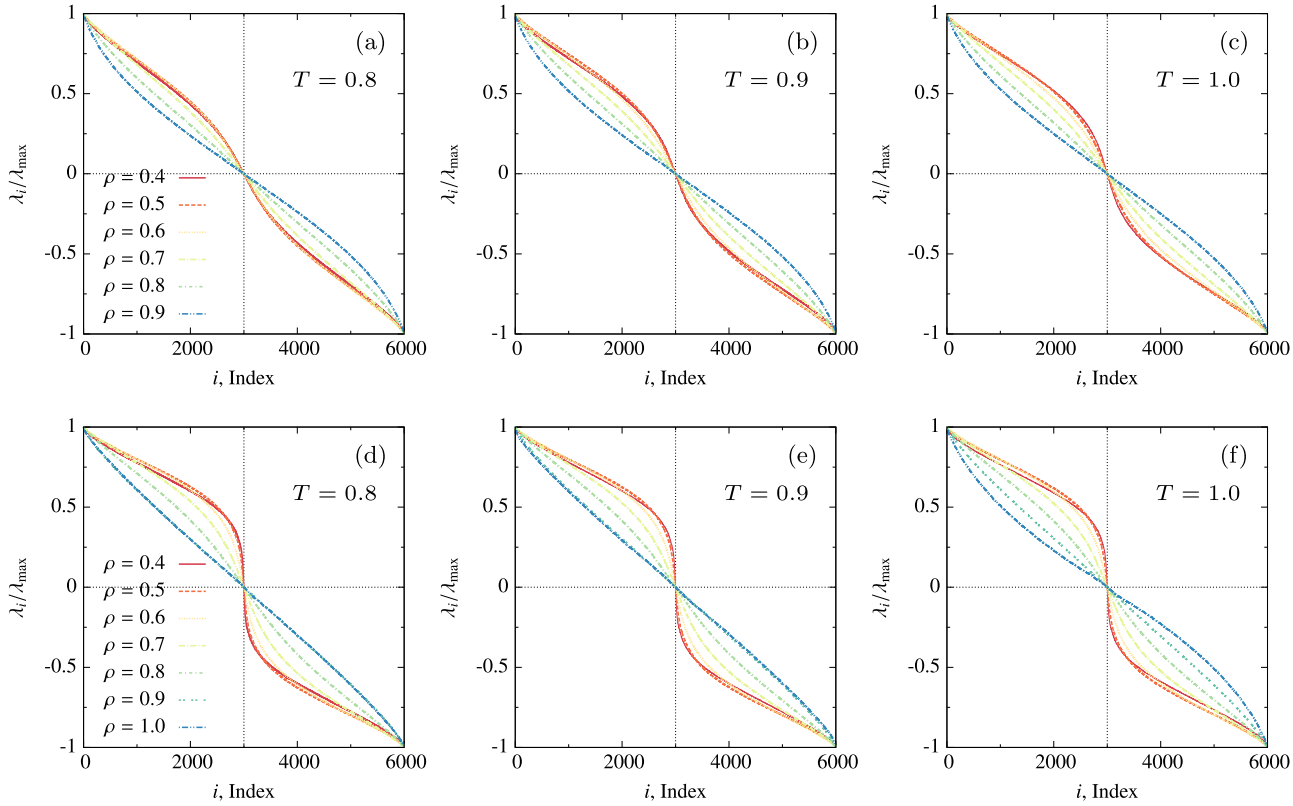

FIG. 7. Normalized Lyapunov spectra, λ_i/λ_{max}, for the (a–c) LJ and (d–f) WCA fluid at densities between 0.4 and 0.9 and between 0.4 and 1.0, respectively, and kinetic temperatures (a, d) $T = 0.8$, (b, e) $T = 0.9$, and (c, f) $T = 1.0$. The number of particles is fixed, $N = 1000$.

C. Density dependence of the Lyapunov spectrum and the KS entropy

Density, like temperature, impacts the Lyapunov instability of simple fluids. Again, the effect depends on the nature of the interparticle interactions. Loosely speaking, density determines the extent of interparticle interaction and particle mobility in the system. Previous studies of simple fluids have measured λ_{max} as a function of density in both two and three dimensions [37,39,43]. However, the KS entropy has been given more attention in two dimensions, presumably because of the challenge of computing the full Lyapunov spectra for high-dimensional systems [37,39]. In these studies, the systems were composed of a small number of particles; the largest system being of the order of hundreds. For example, the extensivity of the KS entropy does not seem to have been fully demonstrated. Furthermore, the only three-dimensional data available for λ_{max} against density is for the LJ fluid. These results, though important, are not exhaustive and motivated us to examine the effect of density on the value of the maximum Lyapunov exponent and the KS entropy for both the WCA and LJ fluids in three-dimensions with a considerably larger number of particles. In large part, this is enabled by our recent work extending the length and time scales of Lyapunov vector calculations [48].

For a fixed number of particles, $N = 1000$, we systematically varied the density of the LJ and WCA fluids in order to analyze the effect on the Lyapunov spectrum and the KS entropy. All initial configurations for the NVE trajectories are samples from a NVT simulation at the appropriate density for both the LJ and WCA systems. The Lyapunov spectra, normalized by λ_{max}, for a range of densities and three temperatures are shown in Figs. 7(a)–7(c) for the LJ fluid and Figs. 7(d)–7(f) for the WCA fluid. For both fluids, the spectrum is concave at low densities and convex at high densities, passing through a linear structure at an intermediate density. Clearly, the spectra are highly sensitive to density: both λ_{max} and h_{KS} exhibit a single maximum in the density range of $\rho = 0.4$–1.1. The location of the maximum depends on temperature for the LJ fluid. Data for three select temperatures is shown in Figs. 8(a) and 8(b). Both dynamical observables also have a maximum for the WCA fluid [Figs. 8(c) and 8(d)]. For a given temperature, though, the location of the maxima for the LJ and WCA fluids differ. Similar trends have been observed for two-dimensional fluids [37,39]. In both fluids, raising the temperature speeds up the divergence of trajectories and, concomitantly, λ_{max} and h_{KS}. These data also explain the observed density dependence of the λ_{max} and h_{KS} against T shown earlier (Fig. 3).

In thermodynamics, increasing density or decreasing volume will decrease the entropy of the system. Intuitively, a smaller volume or higher density suppresses the freedom of particles to collectively exhibit "randomness," which lowers the entropy. Dynamically, though, we observe that increasing the density affects the "dynamical randomness," as measured by h_{KS}, but not monotonically: the KS entropy has a maximum as a function of density. Maxima were also observed in earlier studies of two-dimensional systems [37,39]. For WCA, these investigations suggested the maximum is approximately 20%

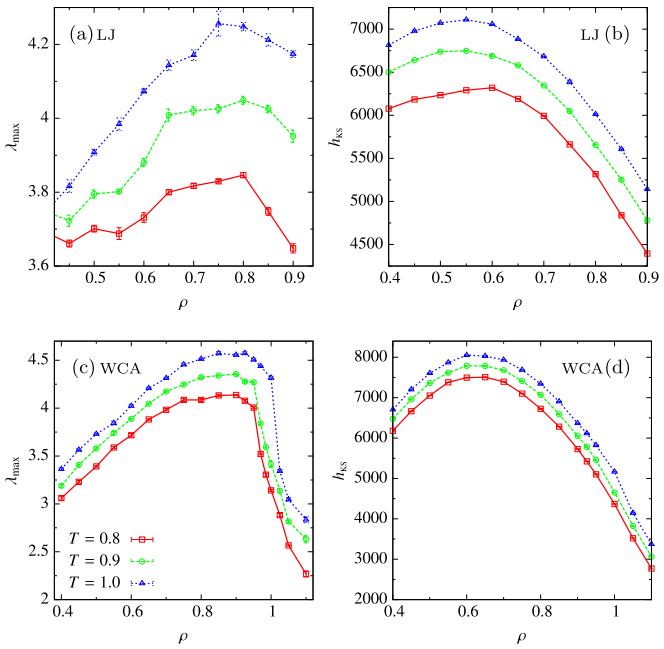

FIG. 8. The dependence of (a) λ_{max} and (b) h_{KS} on the number density ρ at three temperatures for the LJ fluid with $N = 1000$ particles. The dependence of (c) λ_{max} and (d) h_{KS} on ρ for the WCA fluid at the same three temperatures and $N = 1000$.

below the liquid-line density marking the fluid-to-solid phase transition. It is interesting that the most efficient phase-space mixing occurs before, rather than at, the phase boundary [29]. For our data on the LJ fluid, for example, the maximum of h_{KS} appears at points on the phase diagram that are near the liquid-vapor coexistence line. This finding, however, is consistent with currently available data [37,39].

Reference [37] suggests that for the LJ system the maximum of KS entropy occurs at a density that is either in the crystalline solid-vapor coexistence regime (for lower temperature) or above the critical point (for higher temperature) [61]. Here, we observe the maxima in the h_{KS} versus ρ at slightly lower ρ values compared to those found previously for both the LJ and WCA fluids. For the LJ fluid, the density corresponding to the maximum of h_{KS} lies in the liquid-vapor coexistence regime for all three temperatures and this density does not maintain the same difference with the liquid-line density at solid-liquid phase transition for all three temperatures. We observe the maxima in the λ_{max} versus ρ at the same density value for the LJ system but at a somewhat higher ρ value for the WCA fluid than reported in previous studies involving two-dimensional systems [37,39]. It has been suggested that the maximum of h_{KS} involving the onset of phase-transition is a dynamical signature of a nearby phase boundary [37]. However, there is neither an intuitive explanation for why phase space mixing is most efficient prior to the phase boundary nor the initial rise of the KS entropy with density. To confirm the maximum is not a finite-size effect that shifts to the phase boundary in the limit $N \to \infty$, we ran a separate set of simulations for LJ and WCA with $N = 500$. Neither the maxima of the largest exponent nor the maxima of the KS entropy depend on N, which suggests they are not simply a consequence of simulating finite systems.

The maxima in the Lyapunov exponent and KS entropy seem to be a prescient dynamical signature of the nearby phase boundary [61]. A simpler explanation, though, is the competition between two factors: increasing density both shrinks the free volume of the system and increases the average repulsion between the constituent particles [53]. First, the repulsive interaction between the particles makes initially nearby trajectories diverge more rapidly than the attractive interactions, leading to a higher value of λ_{max} and the KS entropy. Evidence of this point also comes from the scaling of h_{KS} with N for the WCA fluid, which shows the KS entropy has a greater magnitude for the WCA fluid than the LJ fluid. The difference between the KS entropies depends on the number of particles, and, hence, the number of repelling pairs. Second, increasing density lowers the free volume and the magnitude of λ_{max} and h_{KS}. These two opposing effects on the value of the maximum exponent and KS entropy could manifest as a turnover in the λ_{max} and h_{KS} versus ρ plot. We hypothesize these factors are the origin of the maxima.

To test our hypothesis, we varied σ for both the LJ and WCA fluid with 1000 particles and examined the fixed-temperature variation of λ_{max} and KS entropy with density. Varying σ also changed the cutoff ($r_c = 2.5\sigma$ for LJ and $r_c = 2^{1/6}\sigma$ for WCA). The parameter σ is the distance between a pair of particles where the attractive and repulsive forces exactly cancel such that $V(\sigma) = 0$. It is a measure of the size of the particles in both the LJ and WCA fluid. Increasing particle size through σ at fixed total volume decreases the free volume, where the free volume is defined as the difference of the entire volume of the simulation box and the volume occupied by the total number of spherical particles. We confirmed through an independent set of simulations that the cutoff does not significantly affect the variation of λ_{max} and h_{KS} against ρ. Therefore, their behavior is solely the effect of σ. As an aside, there is an upper limit on the density we can simulate with increasing σ. At sufficiently high density (high σ), particles cannot diffuse and the fluid becomes structurally arrested. Thus, we concentrate on the density range up to which the system is a fluid.

Both λ_{max} and the KS entropy decrease with increasing particle size at each density for the LJ fluid [Figs. 9(a) and 9(b)]. The maxima of λ_{max} and h_{KS} also shift to smaller density values upon increasing σ. For σ values 1.0 and 1.1, the maximum of λ_{max} occurs at $\rho = 0.8$ and $\rho = 0.6$, respectively, and for $\sigma = 1.25$ the maximum is below $\rho = 0.4$. The maximum of h_{KS} is at $\rho = 0.55$ and $\rho = 0.45$, for $\sigma = 1.0$ and 1.1, respectively, and for $\sigma = 1.25$ it is below $\rho = 0.4$. These results suggest that upon increasing density, the largest exponent and the KS entropy are dominated by the excluded volume and inhibited particle mobility, rather than the number of repulsive pairs, at lower densities and higher σ. We confirmed that these data collapse upon converting these quantities to reduced units (e.g., $\rho\sigma^3$).

The effect of varying σ on the WCA fluid [Figs. 9(c) and 9(d)] differs from the LJ fluid. The difference is greatest at low densities where λ_{max} and h_{KS} do not necessarily show clear trends with σ. The effect on the LJ and WCA fluid is similar at higher densities, however. Increasing σ lowers the available volume, for a fixed total, but it also modifies the extent and nature of repulsions as well. Increasing σ from 1.00 to 1.25

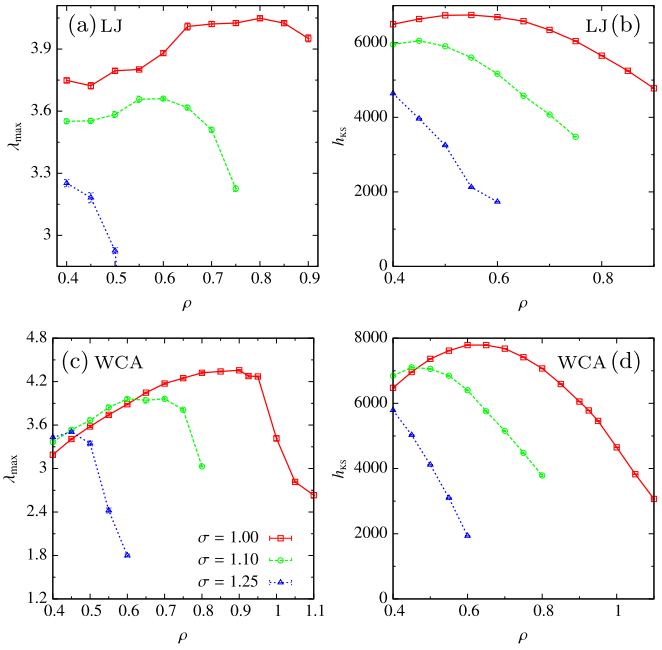

FIG. 9. Dependence of (a) λ_{max} and (b) h_{KS} on the number density, ρ, at $\sigma = 1.00$, 1.10, and 1.25 for the LJ fluid. Dependence of (c) λ_{max} and (d) h_{KS} with ρ at the same σ for the WCA fluid. The number of particles is fixed at $N = 1000$ and the temperature is $T = 0.9$. The density range only includes simulations where the systems are in the fluid phase. For σ values 1.1 and 1.25, the ρ values up to which the system remains in the fluid phase are 0.75 and 0.55, respectively, for both LJ and WCA fluids. In these data, the units of h_{KS} and ρ are not reduced.

makes the repulsive wall of the WCA potential steeper. As only repulsive forces operate in the WCA fluid, repulsions dominate when the influence of excluded volume on λ_{max} and h_{KS} is minimal. For example, at lower densities, where the excluded volume plays a smaller role, we see higher λ_{max} and h_{KS} for higher σ for the WCA fluid. In the case of the WCA fluid, the maxima of λ_{max} and h_{KS} shift toward lower density upon increasing the size of the particles, which indicates that the role of excluded volume starts to become more effective in the low-density domain for higher values of σ. We find that $\rho = 0.9, 0.6$, and 0.45 correspond to the maximum of λ_{max} for $\sigma = 1.0$, 1.1, and 1.25, respectively, and the maximum of h_{KS} appears at $\rho = 0.6$ and $\rho = 0.45$ for σ values 1.0 and 1.1, respectively, whereas it is below $\rho = 0.4$ for $\sigma = 1.25$.

The maxima in λ_{max} and h_{KS} against ρ seem to reflect the competition between free volume per particle and the mean number of repulsive interactions per particle. We quantify the extent of the repulsive forces by the average number of particles, $\langle N_r \rangle$, within a cutoff distance of $2^{1/6}\sigma$ (where the average is over all particles in the fluid). The distance $2^{1/6}\sigma$ corresponds to equilibrium distance between a pair of LJ particles and the distance between WCA particles where they no longer repel. In either case, up to this distance a pair of particles will be repulsive. For a given particle, we measure the number of its neighbors within a sphere of radius $2^{1/6}\sigma$, and average over both the total number of particles (here $N = 1000$) and the time during which the trajectory evolves to calculate $\langle N_r \rangle$. We estimate the free volume per particle,

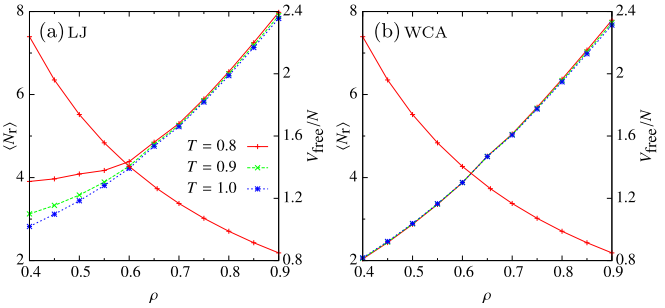

FIG. 10. (a) Average number of repelling particles $\langle N_r \rangle$ and the free volume per particle V_{free}/N as a function of ρ for the LJ fluid at three different temperatures. (b) Variation of $\langle N_r \rangle$ and V_{free}/N against ρ for systems with WCA interaction potential at three different temperatures. (c) Variation of average potential energy and V_{free}/N against ρ for WCA fluid at three different temperatures. The number of particles has been kept fixed at $N = 1000$.

V_{free}/N, from the total volume of the simulation box V and the total excluded volume, using $\sigma/2$ as the radius of each particle. Mathematically, V_{free} is

$$V_{free} = V - \frac{2}{3}N\pi\left(\frac{\sigma}{2}\right)^3. \quad (4)$$

Both $\langle N_r \rangle$ and V_{free} depend on density, the free volume decreasing and the number of repulsions increasing with increasing density as shown in Figs. 10(a) and 10(b) at three different temperatures for both LJ and WCA fluids. In all of these cases, we see this measure of repulsions and the available volume per particle cross at an intermediate density. This numerical evidence qualitatively explains the maxima in the variation of λ_{max} and h_{KS} against ρ.

The mean number of repelling particles $\langle N_r \rangle$ only weakly varies with temperature for intermediate to high-density values for the LJ system and is almost invariant with respect to temperature for the WCA fluid. We find that as a function density $\langle N_r \rangle$ crosses V_{free}/N at nearly the same density at $T = 0.8$, 0.9, and 1.0 for the WCA fluid. The density corresponding to this crossover agrees with the position of the maxima of λ_{max} and h_{KS} against density, which is also not strongly dependent on temperature for the LJ and WCA fluid. Varying σ [Figs. 11(a) and 11(b)] also supports the trends shown in Fig. 9. For LJ and WCA fluids, the crossover regions

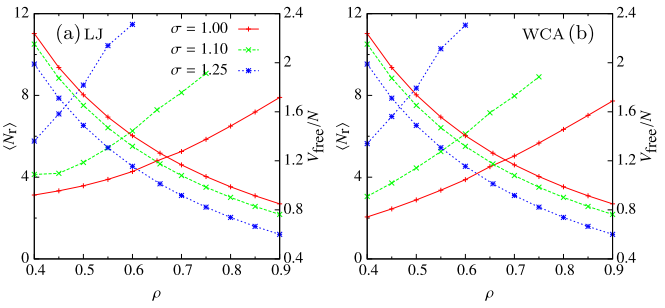

FIG. 11. Average number of repelling particles $\langle N_r \rangle$ and the free volume per particle V_{free}/N as a function of ρ at $\sigma = 1.00$, 1.10, and 1.25 for the (a) LJ and (b) WCA fluid. The number of particles is $N = 1000$ and the kinetic temperature is $T = 0.9$.

for both the $\langle N_r \rangle$ with V_{free}/N shift toward lower densities upon increasing σ. This finding supports the similar shift in the density values corresponding to the maxima of λ_{max} and h_{KS} for greater values of σ in Fig. 9. Overall, these results qualitatively support the turnover in λ_{max} and h_{KS} with ρ being the competition of repulsions and free volume.

IV. CONCLUSIONS

The Lyapunov spectra and KS entropy from dynamical systems theory have long been observables of interest for statistical mechanics. Leveraging recent computational progress, we showed the KS entropy is linearly extensive in, and an additive function of, the number of particles for atomistic models of simple fluids. From our molecular dynamics simulations, these properties hold for both three-dimensional LJ and WCA fluids at several densities and temperatures. At sufficiently high densities, the linear structure of the Lyapunov spectrum gives a geometrical relation that justifies the linear extensivity of the KS entropy. While the extensivity is robust, the structure of the spectrum is not always linear, the exact form being sensitively dependent on the temperature, density, and the nature of the interparticle forces. Because of the intensive nature of λ_{max}, this structure vanishes in the thermodynamic limit: macroscopic simple fluids will have an effectively uniform Lyapunov exponent spectra at equilibrium. Our simulations also showed that the properties of these dynamical observables are a consequence of populations of particles sampling the interaction potential, and that the role of these interparticle forces in the chaotic dynamics agree with the van der Waals picture of fluids—the divergence of trajectories and the magnitude of the KS entropy are dominated by repulsive forces, while attractive forces play a more minor role suppressing the divergence of trajectories.

A more focused study of the effects of temperature on the Lyapunov instability of these fluids shows that λ_{max} and h_{KS} are monotonic functions of temperature. For the WCA fluid, both quantities scale as $\sqrt{T}$, but the temperature range over which Lennard-Jones systems are homogeneous is too narrow to distinguish between T and $\sqrt{T}$ scaling. The monotonic increase with the temperature in these cases, however, agrees qualitatively with the thermodynamic entropy. In contrast, the variation of λ_{max} and the KS entropy with density are nonmonotonic, exhibiting maxima in agreement with previous studies of two-dimensional fluids [37,39]. The appearance of the maxima seems to be the result of the interplay of two opposing factors: the enhancement from repulsive forces and the reduction from the available volume with increasing density. This characteristic variation of the KS entropy with density is in contrast to the thermodynamic entropy for simple fluids. Overall, these equilibrium properties of the KS entropy suggest that it has some features in common with the thermodynamic entropy and others that are unique to its dynamical nature.

ACKNOWLEDGMENTS

Acknowledgment is made to the donors of the American Chemical Society Petroleum Research Fund for support of this research (ACS PRF# 55195-DNI6). We acknowledge the use of the supercomputing facilities managed by the Research Computing Group at the University of Massachusetts Boston as well as the University of Massachusetts Green High Performance Computing Cluster.

[1] C. Jarzynski, Diverse phenomena, common themes, Nat. Phys. **11**, 105 (2015).
[2] J. R. Dorfman, *An Introduction to Chaos in Nonequilibrium Statistical Mechanics* (Cambridge University Press, Cambridge, UK, 1999).
[3] P. Gaspard, *Chaos, Scattering, and Statistical Mechanics* (Cambridge University Press, Cambridge, UK, 1998).
[4] A. N. Kolmogorov, Entropy per unit time as a metric invariant of automorphisms, Dokl. Akad. Nauk. SSSR **124**, 754 (1959).
[5] Ya. G. Sinai, On the concept of entropy for a dynamical system, Dokl. Akad. Nauk. SSSR **124**, 768 (1959).
[6] Y. B. Pesin, Lyapunov characteristic indexes and ergodic properties of smooth dynamic-systems with invariant measure, Dokl. Akad. Nauk. SSSR **226**, 774 (1976).
[7] J.-P. Eckmann and D. Ruelle, Ergodic theory of chaos and strange attractors, Rev. Mod. Phys. **57**, 617 (1985).
[8] N. S. Krylov, *Works on the Foundations of Statistical Physics* (Princeton University Press, Princeton, NJ, 1979).
[9] D. J. Evans and D. J. Searles, The fluctuation theorem, Adv. Phys. **51**, 1529 (2002).
[10] P. Gaspard, Temporal ordering of nonequilibrium fluctuations as a corollary of the second law of thermodynamics, C. R. Phys. **8**, 598 (2007).
[11] P. Gaspard and G. Nicolis, Transport Properties, Lyapunov Exponents, and Entropy Per Unit Time, Phys. Rev. Lett. **65**, 1693 (1990).
[12] R. C. Tolman, The measurable quantities of physics, Phys. Rev. **9**, 237 (1917).
[13] H. Touchette, When is a quantity additive, and when is it extensive? Physica A **305**, 84 (2002).
[14] C. Beck and F. Schlogl, *Thermodynamics of Chaotic Systems* (Cambridge University Press, Cambridge, 1993).
[15] V. Lecomte, C. Appert-Rolland, and F. van Wijland, Chaotic Properties of Systems with Markov Dynamics, Phys. Rev. Lett. **95**, 010601 (2005).
[16] D. J. Searles, D. J. Evans, and D. J. Isbister, The number dependence of the maximum Lyapunov exponent, Physica D **240**, 96 (1997).
[17] D. J. Wales and R. S. Berry, Local interpretation of chaotic dynamics in a many-body classical Hamiltonian system, J. Phys. B: At. Mol. Opt. Phys. **24**, L351 (1991).
[18] M. H. Ernst, J. R. Dorfman, R. Nix, and D. Jacobs, Mean-Field Theory for Lyapunov Exponents and Kolmogorov-Sinai Entropy in Lorentz Lattice Gases, Phys. Rev. Lett. **74**, 4416 (1995).

[19] H. van Beijeren, J. R. Dorfman, H. A. Posch, and Ch. Dellago, Kolmogorov-Sinai entropy for dilute gases in equilibrium, Phys. Rev. E **56**, 5272 (1997).
[20] R. Livi, A. Politi, and S. Ruffo, Distribution of characteristic exponents in the thermodynamic limit, J. Phys. A: Math. Gen. **19**, 2033 (1986).
[21] H. W. Xi, R. Toral, J. D. Gunton, and M. I. Tribelsky, Extensive chaos in the Nikolaevskii model, Phys. Rev. E **62**, R17 (2000).
[22] M. Dzugutov, E. Aurell, and A. Vulpiani, Universal Relation Between the Kolmogorov-Sinai Entropy and the Thermodynamical Entropy in Simple Liquids, Phys. Rev. Lett. **81**, 1762 (1998).
[23] E. G. D. Cohen and L. Rondoni, Comment on "Universal Relation Between the Kolmogorov-Sinai Entropy and the Thermodynamical Entropy in Simple Liquids," Phys. Rev. Lett. **84**, 394 (2000).
[24] M. Dzugutov, Dzugutov Replies, Phys. Rev. Lett. **84**, 395 (2000).
[25] V. Latora and M. Baranger, Kolmogorov-Sinai Entropy Rate Versus Physical Entropy, Phys. Rev. Lett. **82**, 520 (1999).
[26] A. Samanta, Sk. M. Ali, and S. K. Ghosh, New Universal Scaling Laws of Diffusion and Kolmogorov-Sinai Entropy in Simple Liquids, Phys. Rev. Lett. **92**, 145901 (2004).
[27] T. Taniguchi and G. P. Morriss, Stepwise structure of Lyapunov spectra for many-particle systems using a random matrix dynamics, Phys. Rev. E **65**, 056202 (2002).
[28] C. Forster, R. Hirschl, H. A. Posch, and W. G. Hoover, Perturbed phase-space dynamics of hard-disk fluids, Physica D **187**, 294 (2004).
[29] J. A. van Meel and H. A. Posch, Lyapunov instability of rough hard-disk fluids, Phys. Rev. E **80**, 016206 (2009).
[30] Ch. Dellago, Ch. Dellago, H. A. Posch, and W. G. Hoover, Lyapunov instability in a system of hard disks in equilibrium and nonequilibrium steady states, Phys. Rev. E **53**, 1485 (1996).
[31] Ch. Dellago and H. A. Posch, Kolmogorov-Sinai entropy and Lyapunov spectra of a hard-sphere gas, Physica A **240**, 268 (1997).
[32] A. S. de Wijn and H. van Beijeren, Goldstone modes in Lyapunov spectra of hard sphere systems, Phys. Rev. E **70**, 016207 (2004).
[33] A. S. de Wijn, Kolmogorov-Sinai entropy for dilute systems of hard particles in equilibrium, Phys. Rev. E **71**, 046211 (2005).
[34] H. Bosetti and H. A. Posch, What does dynamical systems theory teach us about fluids? Commun. Theor. Phys. **62**, 451 (2014).
[35] H. A. Posch and Wm. G. Hoover, Lyapunov instability of classical many-body systems, J. Phys. Conf. Ser. **31**, 9 (2006).
[36] Wm. G. Hoover, H. A. Posch, C. Forster, Ch. Dellago, and M. Zhou, Lyapunov modes of two-dimensional many-body systems; soft disks, hard disks, and rotors, J. Stat. Phys. **109**, 765 (2002).
[37] Ch. Dellago and H. A. Posch, Lyapunov instability, local curvature, and the fluid-solid phase transition in two-dimensional particle systems, Physica A **230**, 364 (1996).
[38] W. G. Hoover and H. A. Posch, Second-law irreversibility and phase-space dimensionality loss from time-reversible nonequilibrium steady state Lyapunov spectra, Phys. Rev. E **49**, 1913 (1994).
[39] Ch. Forster and H. A. Posch, Lyapunov modes in soft-disk fluids, New J. Phys. **7**, 32 (2005).
[40] W. G. Hoover and H. A. Posch, Shear viscosity via global control of spatiotemporal chaos in two-dimensional isoenergetic dense fluids, Phys. Rev. E **51**, 273 (1995).
[41] H. Yang and G. Radons, Lyapunov instabilities of Lennard-Jones fluids, Phys. Rev. E **71**, 036211 (2005).
[42] H. A. Posch and W. G. Hoover, Lyapunov instability of dense Lennard-Jones fluids, Phys. Rev. A **38**, 473 (1988).
[43] H. A. Posch, W. G. Hoover, and B. L. Holian, Time reversible molecular motion and microscopic irreversibility, Ber. Bunsenges. Phys. Chem. **94**, 250 (1990).
[44] H. A. Posch and W. G. Hoover, Equilibrium and nonequilibrium Lyapunov spectra of dense fluids and solids, Phys. Rev. A **39**, 2175 (1989).
[45] D. Ihm, Y. Shin, J. Lee, and E. K. Lee, Correlation between Kolmogorov-Sinai entropy and self-diffusion coefficient in simple fluids, Phys. Rev. E **67**, 027205 (2003).
[46] S. Sastry, Lyapunov Spectra, Instantaneous Normal Mode Spectra, and Relaxation in the Lennard-Jones Liquid, Phys. Rev. Lett. **76**, 3738 (1996).
[47] T. L. Beck, D. M. Leitner, and R. S. Berry, Melting and phase space transitions in small clusters: Spectral characteristics, dimensions, and K-entropy, J. Chem. Phys. **89**, 1681 (1988).
[48] A. B. Costa and J. R. Green, Extending the length and time scales of Gram-Schmidt Lyapunov vector computation, J. Comput. Phys. **246**, 113 (2013).
[49] D. Frenkel and B. Smit, *Understanding Molecular Simulation* (Academic Press, London, 1996).
[50] J. P. Hansen and J. R. McDonald, *Theory of Simple Liquids* (Academic Press, New York, 2005), 3rd ed.
[51] T. S. Ingebrigtsen, T. B. Schrøder, and J. C. Dyre, What is a Simple Liquid? Phys. Rev. X **2**, 011011 (2012).
[52] J. E. Jones, On the determination of molecular fields, Proc. R. Soc. A **106**, 463 (1924).
[53] J. D. Weeks, D. Chandler, and H. C. Andersen, Role of repulsive forces in determining the equilibrium structure of simple liquids, J. Chem. Phys. **54**, 5237 (1971).
[54] S. D. Stoddard and J. Ford, Numerical experiments on the stochastic behavior of a Lennard-Jones gas system, Phys. Rev. A **8**, 1504 (1973).
[55] H. Fujisaka, Statistical dynamics generated by fluctuations of local Lyapunov exponents, Prog. Theor. Phys. **70**, 1264 (1983).
[56] G. Benettin, L. Galgani, A. Giorgilli, and J.-M. Strelcyn, Lyapunov characteristic exponents for smooth dynamical systems and for Hamiltonian systems a method for computing all of them. Part 1: Theory, Meccanica **15**, 9 (1980).
[57] J. R. Green, A. B. Costa, B. A. Grzybowski, and I. Szleifer, Relationship between dynamical entropy and energy dissipation far from thermodynamic equilibrium, Proc. Natl. Acad. Sci. USA **110**, 16339 (2013).
[58] J. R. Green, J. Jellinek, and R. S. Berry, Space-time properties of Gram-Schmidt vectors in classical Hamiltonian evolution, Phys. Rev. E **80**, 066205 (2009).
[59] R. J. Hinde, R. S. Berry and D. J. Wales, Chaos in small clusters of inert-gas atoms, J. Chem. Phys. **96**, 1376 (1992).
[60] D. J. Albers, J. C. Sprott, and J. P. Crutchfield, Persistent chaos in high dimensions, Phys. Rev. E **74**, 057201 (2006).
[61] B. Smit, Phase diagrams of Lennard-Jones fluids, J. Chem. Phys. **96**, 8639 (1992).
[62] F. Calvo, Largest Lyapunov exponent in molecular systems: Linear molecules and application to nitrogen clusters,

Phys. Rev. E **58**, 5643 (1998); Largest Lyapunov exponent in molecular systems. II: Quaternion coordinates and application to methane clusters, *ibid.* **60**, 2771 (1999).

[63] J. R. Green, T. S. Hofer, D. J. Wales, and R. S. Berry, Chaotic dynamics near steep transition states, Mol. Phys. **110**, 1839 (2012).

[64] J. R. Green, T. S. Hofer, R. S. Berry, and D. J. Wales, Characterizing molecular motion in H_2O and H_3O^+ with dynamical instability statistics, J. Chem. Phys. **135**, 184307 (2011).

[65] S. Sarman, D. J. Evans, and G. P. Morriss, Conjugate-pairing rule and thermal-transport coefficients, Phys. Rev. A **45**, 2233 (1992).